

Quantum phase transition in the anisotropic Rabi model induced by parametric amplification

Yuan Qiu,^{1,2} Ke-Xiong Yan,^{1,2} Jun-Hao Lin,^{1,2} Jie Song,³ Ye-Hong Chen,^{1,2,4,*} and Yan-Xia^{1,2,†}

¹*Fujian Key Laboratory of Quantum Information and Quantum Optics, Fuzhou University, Fuzhou 350116, China*

²*Department of Physics, Fuzhou University, Fuzhou, 350116, China*

³*Department of Physics, Harbin Institute of Technology, Harbin 150001, China*

⁴*Quantum Information Physics Theory Research Team,*

Center for Quantum Computing, RIKEN, Wako-shi, Saitama 351-0198, Japan

(Dated: November 6, 2025)

In this manuscript, we analyze the mechanism of the superradiant phase transition in the anisotropic Rabi model under the classical oscillator limit using the pattern picture. By expanding the anisotropic Rabi model Hamiltonian in operator space, we obtained three patterns, and we find that the phase transition arises from the competition between patterns. The difficulty in achieving the classical oscillator limit motivates our investigation into the quantum phase transition within a parametrically-driven Jaynes-Cummings model. This parametrically-driven Jaynes-Cummings model can reproduce the dynamics of a ultrastrong-coupling anisotropic Rabi model in a squeezed-light frame. According to the eigenenergies and eigenstates of the normal and superradiant phases of this equivalent anisotropic Rabi model, we find that the excitation energy of the normal phase and the superradiant phase vanishes at the critical point. The photon number becomes infinite beyond the critical point. These results indicate that the system undergoes a superradiant phase transition at the critical point.

I. INTRODUCTION

Since 1937, Landau and Ginzburg proposed a universal method for dealing with phase transition by introducing the concept of order parameter, the study of modern phase transitions and critical behavior has formed a mature theoretical framework [1, 2]. When the coupling strength reaches a critical value, phenomena such as macroscopic occupancy of photons and abrupt changes in the system's ground state indicate the occurrence of quantum phase transition (QPT) [3–6]. QPT has become one of the core topics in condensed matter physics [7–9] and quantum optics [10, 11], due to its characteristic of being dominated by quantum fluctuations at absolute zero, and has been widely studied in various light-matter coupling systems, such as the Dicke-type system [12–20]. The Dicke-type system describes the interaction between a single-mode boson field and an ensemble of N two-level atoms, which exhibits a superradiant phase transition at thermodynamic limits, i.e. $N \rightarrow \infty$ [12, 21–25].

However, reaching the thermodynamic limit is one of the main challenges in achieving QPT in laboratories [4]. This challenge has prompted researchers to turn their attention to the study of the QPT in finite-sized systems, such as the quantum Rabi model [3, 26–32], which is a simplified version of the Dicke model with $N = 1$. In this model, the classical oscillator limit (i.e., the ratio of atomic transition frequency ω_q to cavity field frequency ω_c approaches infinity) replaces the thermodynamic limit and also theoretically

predicts the QPT [33]. The anisotropic Rabi model can be defined as the generalization of the spin-boson Rabi model [34], unlike the standard quantum Rabi model, the anisotropic Rabi model has different coupling strengths for the rotating-wave and counterrotating-wave interaction terms [35]. Previous studies have shown that this model also undergoes a phase transition in the classical oscillator limit [31]. However, the physical mechanism responsible for this phase transition has not been thoroughly studied.

In this manuscript, we diagonalize the anisotropic Rabi model Hamiltonian in the operator space, gaining a deeper understanding of the reasons for the occurrence of QPT in the anisotropic Rabi model. The results show that there is a competitive relationship among the three patterns in the superradiant phase transition, which explains why and how the superradiant phase transition occurs. We also discuss the influence of varying ratios of the coupling strengths of the rotating-wave term and counter-rotating-wave term on pattern competition. Regarding the difficulty of reaching the classical oscillator limit in quantum phase transition and the challenges posed by the no-go theorem [33, 36–39], we apply a parametric amplification method in a generic cavity quantum electrodynamics system to obtain a simulated anisotropic Rabi model to explore the QPT. Specifically, we apply a two-photon drive in the Jaynes-Cummings (JC) model [40–45] to obtain a simulated anisotropic Rabi model. The effective cavity frequency and the equivalent coupling of this simulated quantum Rabi model are related to the two-photon drive strength. Therefore, we can control the occurrence of the phase transition by changing the drive strength.

To investigate the critical behavior of this simulated

* yehong.chen@fzu.edu.cn

† xia-208@163.com

anisotropic Rabi model, we derive its effective low-energy Hamiltonian in the classical oscillator limit, and obtain the eigenenergies and eigenstates of the normal phase and the superradiant phase. The simulation results indicate that when the coupling strength approaches the critical point, the system exhibits unique critical behaviors that mark the QPT. Specifically, the excitation energy becomes zero. The ground-state energy is continuous at the critical point, while the second-order derivative of the ground-state energy to the coupling strength is discontinuous at the critical point. When the coupling strength exceeds the critical point, the photon number exhibits macroscopic occupation.

The structure of the manuscript is as follows. In Sec. II we review the key aspects of Ref. [4] on quantum phase transition. In Sec. III we diagonalize the anisotropic Rabi model in the operator space and analyze why and how the phase transition occurs. In Sec. IV present the model and Hamiltonian, and derive the eigenenergies and eigenstates of the normal phase and the superradiant phase. In Sec. V we demonstrate that the simulated anisotropic Rabi model undergoes a phase transition at the critical point, and prove that the occurrence of this transition can be controlled by tuning the squeezing parameter. Finally, we conclude our manuscript in Sec. VI.

II. PHASE TRANSITION IN THE ANISOTROPIC RABI MODEL: PRIOR WORK

The anisotropic Rabi model features unequal coupling strengths for its rotating- and counter-rotating-wave interactions. In Ref. [4], Shen et al. investigated the phase transitions of the anisotropic Rabi model under the classical oscillator limit ($\Omega/\omega_0 \rightarrow \infty$) and the Hamiltonian of the anisotropic Rabi model they studied is denoted as

$$H_{\text{AN}} = \omega_0 a^\dagger a + \frac{\Omega}{2} \sigma_z - \xi_1 (a \sigma_+ + a^\dagger \sigma_-) - \xi_2 (a \sigma_- + a^\dagger \sigma_+). \quad (1)$$

Here, $a^\dagger(a)$ is a creation (annihilation) operator for the harmonic oscillator with the frequency ω_0 , $\sigma_+(\sigma_-)$ and σ_z are Pauli matrices for the qubit with the transition frequency Ω . The parameters ξ_1 and ξ_2 characterize the qubit-oscillator coupling strengths of the rotating-wave and counterrotating-wave interactions, respectively. By projecting the effective Hamiltonians of the normal and superradiant phases onto their corresponding spin-down subspaces, the low-energy effective Hamiltonians for both phases can be obtained.

The low-energy effective Hamiltonian of the normal phase is

$$H_{\text{np}}^{\text{AN}} = (\omega_0 - \frac{\xi_1^2 + \xi_2^2}{\Omega}) a^\dagger a - \frac{\xi_1 \xi_2}{\Omega} (a^{\dagger 2} + a^2) - \frac{\xi_2^2}{\Omega} - \frac{\Omega}{2}. \quad (2)$$

According to the squeezing transformation $S_{\text{AN}}^\dagger(r_{\text{AN}}) H_{\text{np}}^{\text{AN}} S_{\text{AN}}(r_{\text{AN}})$, where $S_{\text{AN}}(r_{\text{AN}}) = \exp[r_{\text{AN}}(a^{\dagger 2} - a^2)/2]$, when the coefficient of the $(a^{\dagger 2} + a^2)$, the diagonalized Hamiltonian of the normal phase is

$$H_{\text{np}}^{\text{AN}'} = \epsilon_{\text{np}} a^\dagger a + E_{\text{np}}, \quad (3)$$

with the excitation energy,

$$\epsilon_{\text{np}}^{\text{AN}} = \sqrt{(\omega_0 - \frac{\xi_1^2 + \xi_2^2}{2})^2 - (\frac{2\xi_1 \xi_2}{\Omega})^2}, \quad (4)$$

and the the ground-state energy is

$$E_{\text{np}}^{\text{AN}} = \frac{1}{2} (\epsilon_{\text{np}}^{\text{AN}} - \omega_0 + \frac{\xi_1^2 + \xi_2^2}{\Omega} - \Omega). \quad (5)$$

For $\omega_0 > (\xi_1^2 + \xi_2^2)/\Omega$, the excitation energy $\epsilon_{\text{np}}^{\text{AN}}$ is real only when $\omega_0 - (\xi_1^2 + \xi_2^2)/\Omega \geq 2\xi_1 \xi_2/\Omega$, then the critical coupling strength is

$$\xi_c = \frac{\xi_1 + \xi_2}{\sqrt{\omega_0 \Omega}} \leq 1. \quad (6)$$

The eigenstates and eigenenergies of $H_{\text{np}}^{\text{AN}'}$ are

$$|\phi_{\text{np}}^n\rangle = S(r_{\text{np}}) |n\rangle |\downarrow\rangle, \quad (7)$$

$$E_{\text{np}}^n = n\epsilon_{\text{np}} + E_{\text{np}}. \quad (8)$$

For the superradiant phase, its low-energy effective Hamiltonian is

$$H_{\text{sp}}^{\text{AN}} \simeq \omega_0 a^\dagger a - \frac{(\xi_1 + \xi_2)^2 \xi_c^{-4} + (\xi_1 - \xi_2)^2}{2\Omega \xi_c^2} a^\dagger a - \frac{(\xi_1 + \xi_2)^2 \xi_c^{-4} - (\xi_1 - \xi_2)^2}{4\Omega \xi_c^2} (a^{\dagger 2} + a^2) - \frac{(\xi_1 + \xi_2) \xi_c^{-2} - (\xi_1 - \xi_2)}{2\Omega \xi_c^2} - \frac{\Omega}{4} (\xi_c^2 + \xi_c^{-2}) \quad (9)$$

with the excitation energy,

$$\epsilon_{\text{sp}}^{\text{AN}} = \omega_0 \frac{2\sqrt{\xi_1 \xi_2}}{\xi_1 + \xi_2} \sqrt{1 - \xi_c^{-4}}, \quad (10)$$

and the the ground-state energy

$$E_{\text{sp}}^{\text{AN}} = \frac{1}{2} \left(\epsilon_{\text{sp}}^{\text{AN}} - \omega_0 - \frac{\xi_1^2 + \xi_2^2}{\Omega} \right) - \frac{\Omega}{4} (\xi_c^2 + \xi_c^{-2}) - \frac{(\xi_1 + \xi_2) \xi_c^{-2} - (\xi_1 - \xi_2)}{2\Omega \xi_c^2}. \quad (11)$$

The eigenstates and eigenenergies of $H_{\text{sp}}^{\text{AN}}$ are written as

$$|\phi_{\text{sp}}^n\rangle = D(\pm \alpha_0) S(r_{\text{sp}}) |n\rangle |\downarrow^\pm\rangle. \quad (12)$$

Reference [4] further analyzed the excitation energy, ground-state energy, second-order derivative of the

ground-state energy, and photon number in the two-dimensional parameter space (ξ_1, ξ_2) . The numerical results demonstrate that the excitation energies of both the normal and superradiant phases vanish when $\xi_c \rightarrow 1$, the ground-state energy remains continuous at the critical coupling strength while its second derivative exhibits a discontinuity, and the order parameter $\langle a^\dagger a \rangle$ jumps from zero to infinity. These conclusively verified the occurrence of a QPT in the anisotropic Rabi model at the critical coupling strength. The simulation results in a two parameter space uncovered distinctive physical behaviors under the critical conditions of QPT. Specifically, the critical condition in the isotropic Rabi model is a point in a one-dimensional parameter space, but in the anisotropic Rabi model it is a straight line in a two-dimensional parameter space which essentially extends the dimensionality of the QPT.

III. DISSECTING PHASE TRANSITION IN THE ANISOTROPIC RABI MODEL

In Sec. II, we reviewed how Shen et al. successfully characterized the critical behavior of the anisotropic Rabi model using low-energy effective Hamiltonians. However, a microscopic understanding of how competing interactions drive this phase transition remains incomplete. In this section, We diagonalize the Hamiltonian H_{AN} in Eq. (1) in the operator space to obtain three fundamental patterns for dissecting QPT [46]. These three patterns are represented as λ_1, λ_2 and λ_3 , which are exact because they can precisely reproduce the Hamiltonian matrix for a given Fock basis. By using the relation $\sigma_x \sigma_y = i\sigma_z$, the Hamiltonian H_{AN} in Eq. (1) can be reformulated as follows:

$$H_{\text{AR}} = (\sigma_x \ i\sigma_y \ a^\dagger) \begin{pmatrix} 0 & \frac{\Omega}{4} & -\frac{\xi_1+\xi_2}{2} \\ \frac{\Omega}{4} & 0 & \frac{\xi_2-\xi_1}{2} \\ -\frac{\xi_1+\xi_2}{2} & \frac{\xi_2-\xi_1}{2} & \omega_0 \end{pmatrix} \begin{pmatrix} \sigma_x \\ -i\sigma_y \\ a \end{pmatrix} = \sum_{n=1}^3 \lambda_n A_n^\dagger A_n, \quad (13)$$

$$A_n = u_{n,1}(i\sigma_y) + u_{n,2}\sigma_z + u_{n,3}a, \quad (14)$$

where λ_n and u_n ($n = 1, 2, 3$) are the eigenvalues and eigenvectors of the matrix in Eq. (13), respectively. They form three basic patterns represented by eigenstates and eigenvectors, as shown in Fig. 6(a). Before discussing the phase transition with pattern picture, we will first verify the validity of the pattern picture.

A. Patterns and solution

Equation (13) can be solved by expanding the system states in the complete basis $|\Gamma_z, m\rangle$, where

$$\sigma_z |\Gamma_z\rangle = \pm(\uparrow, \downarrow) |\Gamma_z\rangle \quad (15)$$

denotes the spin eigenstate along the z -direction and $a^\dagger a |m\rangle = m|m\rangle$ ($m = 0, 1, 2, \dots, N$) denotes the truncated Fock basis with the photon number m . The matrix elements of A_n in this basis are constructed as

$$[A_n]_{\Gamma_z, m; \Gamma'_z, m'} = \langle \Gamma_z, m | A_n | m', \Gamma'_z \rangle. \quad (16)$$

Subsequently, Eq. (13) can be addressed by diagonalizing the matrix as follows

$$\begin{aligned} \langle \Gamma_z, m | H_{\text{AR}} | m', \Gamma'_z \rangle &= \sum_{n=1}^3 \lambda_n \langle \Gamma_z, m | A_n^\dagger A_n | m', \Gamma'_z \rangle \\ &= \sum_{n=1}^3 \lambda_n \sum_{\Gamma''_z, m''} [A_n]_{m, \Gamma_z; m'', \Gamma''_z} [A_n]_{m'', \Gamma''_z; m', \Gamma'_z}. \end{aligned} \quad (17)$$

Upon obtaining the eigenstate wavefunctions Ψ_i (where $i = 0, 1, \dots$, corresponds to the ground state, the excited state, and so on), these wavefunctions are projected onto different patterns to determine the contributions of these patterns to the target physical quantities. Taking energy as an example, the energy contributions of the three patterns to the eigenstate $|\Psi_i\rangle$ can be calculated by the following equation

$$E_{\lambda_n} = \langle \Psi_i | \lambda_n A_n^\dagger A_n | \Psi_i \rangle, \quad (n = 1, 2, 3). \quad (18)$$

By substituting A_n in Eq. (13) into $\langle \Psi_i | A_n^\dagger A_n | \Psi_i \rangle$, the relevant physical observability can be expressed as $\langle \Psi_i | a^\dagger a | \Psi_i \rangle_{\lambda_n} = u_{n,3}^2 \langle \Psi_i | a^\dagger a | \Psi_i \rangle$, which can be easily calculated after diagonalizing the Hamiltonian matrix as given in Eq. (17) to obtain $|\Psi_i\rangle$.

We know that a dramatic change in energy at the critical point signifies the occurrence of a QPT, which is a well-known result in Ref. [3, 47]. We set $\xi_2 = k\xi_1$, i.e., the coupling strength of the counter-rotating term is k times that of the rotating-wave term. Figs 2(a)–2(c) present the first four energy levels against the k/k_c of the three patterns, where k_c is the value of k when $\xi_c = 1$ in Eq. (6). The energy of all three patterns undergoes a sudden change at the critical point $k/k_c \sim 1$. To verify the validity of the patterns, we compare the results of the sum of the corresponding physical quantities energy E and photon number $\langle a^\dagger a \rangle$ of patterns with those obtained directly by numerical exact diagonalization (ED). Figures 3(a) and 3(b) show sharp changes in both energy levels and photon number near $k/k_c \sim 1$, consistent with the results of the superradiant phase transition demonstrated in Ref. [4]. Moreover, the results of the summations of the patterns exhibit an exact agreement with those obtained through ED.

In Fig. 3, solid lines denote the summed contributions of patterns, while symbols indicate the ED results. This agreement stems from the absence of additional approximations in the pattern picture compared to the ED method. Consequently, this formalism enables a systematic decomposition of the anisotropic quantum Rabi model Hamiltonian into fundamental patterns. Such a decomposition provides a new perspective for

(a) Pattern λ_1			(b) Pattern λ_2			(c) Pattern λ_3		
$i\sigma_x$	$-i\sigma_y$	a	$i\sigma_x$	$-i\sigma_y$	a	$i\sigma_x$	$-i\sigma_y$	a
$u_{1,1}$	$u_{1,2}$	$u_{1,3}$	$u_{2,1}$	$u_{2,2}$	$u_{2,3}$	$u_{3,1}$	$u_{3,2}$	$u_{3,3}$
+	-	+	-	+	+	-	-	+

FIG. 1. Marks of the patterns obtained by diagonalizing the Hamiltonian H_{AN} .

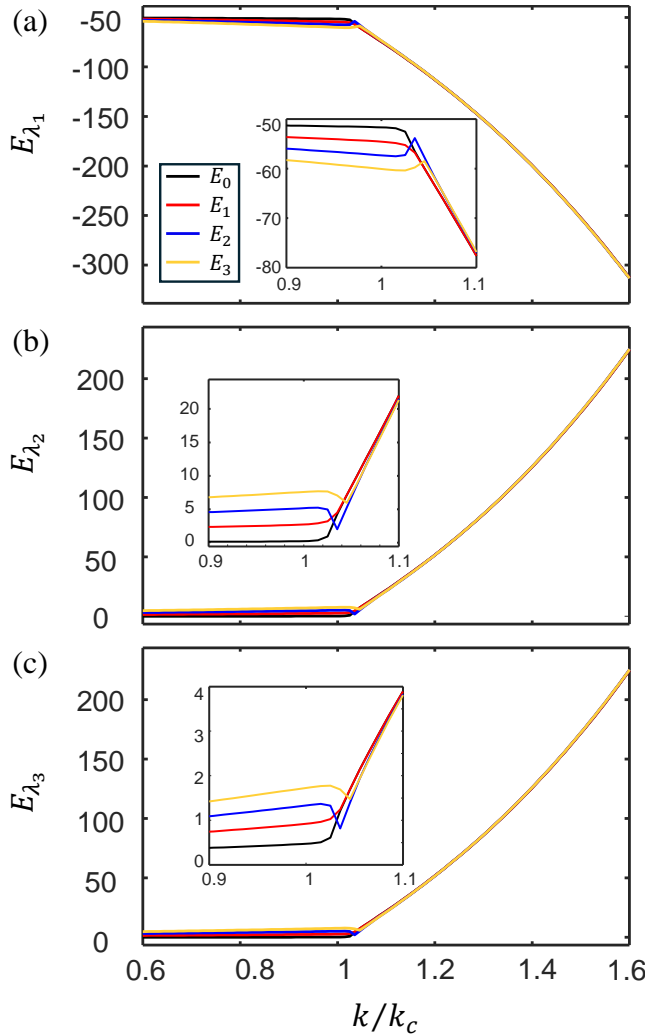


FIG. 2. First four pattern energy levels as a function of k/k_c . The insets show an enlarged region of the k/k_c ranging from 0.9 to 1.1. We set $\Omega = 100\omega_0$ and $\xi_1 = 0.1\omega_0$.

analyzing phenomena in the anisotropic quantum Rabi model, such as the superradiant phase transition central to this manuscript.

B. The properties of phase transition

The anisotropic quantum Rabi model exhibits a superradiant phase transition at the critical ratio $k/k_c \sim 1$, where the energy levels, mean photon number $\langle a^\dagger a \rangle$ undergo abrupt changes, as shown in Fig. 3. These

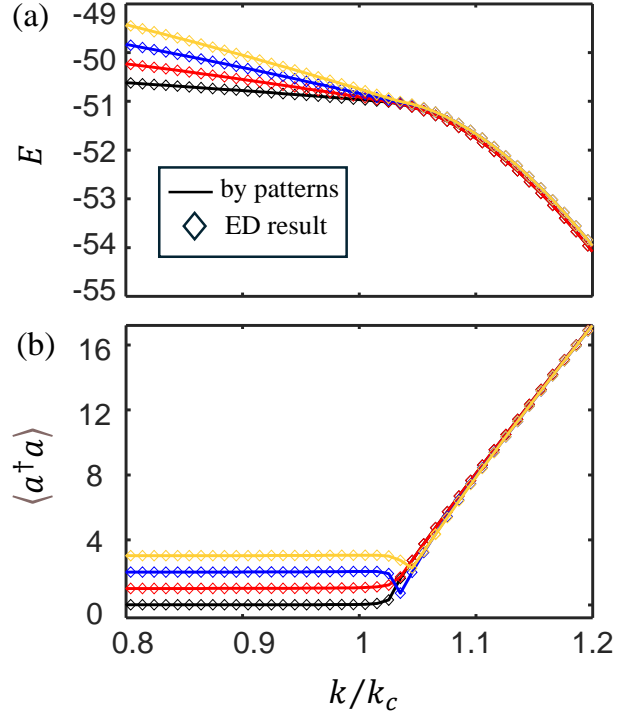


FIG. 3. Comparison between the relevant physical quantities obtained from patterns and those obtained from ED. (a) Summation of patterns energy levels (lines) and their comparison with the results obtained directly by ED (diamond). (b) Comparison of the summations of the patterns' photon number (lines) $\langle a^\dagger a \rangle$ to those obtained by ED (diamond). The parameters are the same as Fig. 2.

abrupt changes are characteristic features of the system's transition from the normal phase to the superradiant phase, which is consistent with the universal critical behavior of light-matter systems near the quantum

critical point [3]. We systematically analyze the origin of the phase transition by quantifying the contributions of distinct patterns to the ground and first excited states. This analysis reveals a competition mechanism among the patterns, and we find that the ratio k influences the competition between patterns.

The upper panel of Fig. 4 corresponds to the contribution of patterns to the energy level of ground state and its second derivative with respect to coupling strength ξ_1 , as a function of ξ_1/ξ_{1c} when $k = 0.9$. As shown in Fig. 4(a1), in the weak-coupling regime (i.e. $\xi_1/\xi_{1c} \leq 1$), the ground state is entirely governed by the dominant pattern λ_1 (red solid line), while contributions from other patterns (λ_2, λ_3) are negligible. This regime corresponds to the well-known normal phase of the anisotropic quantum Rabi model, characterized by a zero photon number. As the coupling strength increases, the system enters the superradiant phase, where the different patterns exhibit the following distinct critical behaviors.

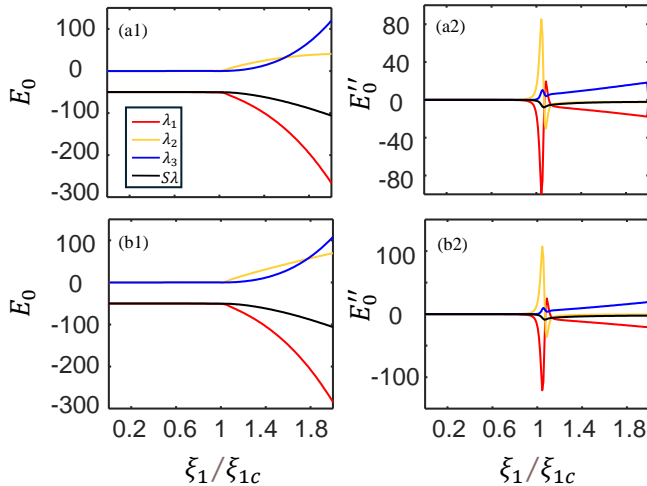


FIG. 4. (a1),(b1) Sum of patterns of ground state energy (black solid line) and corresponding pattern components (red, yellow, and blue solid lines) as as functions of coupling strength ξ_1/ξ_{1c} when $k = 0.9$ and $k = 1$. (a2),(b2) Second-order derivatives of the corresponding energy levels (black solid line) and corresponding pattern components (red, yellow, and blue solid lines).

(i) Descend of λ_1 . The pattern λ_1 experiences a sharp decline followed by a continuous descend. (ii) Compensatory response of λ_2 . The pattern λ_2 exhibits a rapid compensatory growth in response to the decline of λ_1 (iii) Response to the decline of λ_3 . The imbalance between λ_1 and λ_2 triggers the λ_3 , which becomes the primary contributor to stabilize the superradiant phase. This behavior is identical to the competition observed in the lower panels for $k = 1$, corresponding to the isotropic Rabi model. In Fig. 4(a2) and Fig. 4(b2), the second-order derivatives of the contribution of the

pattern λ_1 and the pattern λ_3 show similar changes but opposite trends as the coupling strength ξ/ξ_{1c} increases in the superradiant phase, highlighting the competition between these patterns. The competition between the patterns λ_1 and $\lambda_{2,3}$ elucidates the microscopic mechanism of the superradiant phase transition, i.e., by increasing the coupling strength, the photon number is excited, thereby reducing the energy of the system driven by pattern λ_1 . To counterbalance this energy reduction, the pattern λ_2 and pattern λ_3 generate positive energy contributions, stabilizing the system in the emergent superradiant phase.

However, for $k = 0.5$ and 1.5 , the competition between patterns exhibits different behavior in the superradiant phase. When $k = 0.5$, both patterns λ_1 and λ_2 decrease, with growing coupling strength. At the same time, pattern λ_3 develops a compensatory response that balances their energy reduction [see Fig. 5(a1)]. When $k = 1.5$, as the coupling strength increases, pattern λ_1 exhibits continuous suppression. Pattern λ_2 provides a compensatory response but cannot fully balance the energy reduction caused by pattern λ_1 , making pattern λ_3 becomes crucial for balancing pattern λ_1 , ultimately compensating for its energy loss [see Fig. 5(b1)]. Unlike what is shown in Fig. 4, pattern λ_2 here compensates more energy than pattern λ_1 . The interplay of energy suppression (λ_1) and compensation ($\lambda_{2,3}$) directly manifests the critical competition governing the phase transition, providing a unified framework for understanding the emergence of superradiation phase in anisotropic QRM. Similar phenomena can be observed in the first excited state, as shown in Fig. 6.

The the classical oscillator limit ($\Omega/\omega_0 \rightarrow \infty$) mentioned in Sec. II is crucial for studying quantum phase transitions in the anisotropic Rabi model. However, this limit is experimentally challenging to realize. In the next section, we consider a parametric amplification method in a driven cavity QED system. This method can exponentially enhance the coupling strength and suppress the effective cavity frequency, thereby satisfying the harmonic oscillator limit and enabling the study of anisotropic Rabi model phase transitions under experimentally feasible conditions.

IV. MODEL AND HAMILTONIAN

The system of a qubit weakly coupled to a cavity driven by the two-photon drive can be illustrated as Fig. 7. Working in a frame rotating at half the parametric drive frequency $\omega_p/2$, the Hamiltonian can be written as

$$H = \delta_c a^\dagger a + \frac{\delta_q}{2} \sigma_z - \frac{\eta}{2} (a^{\dagger 2} + a^2) + g(a^\dagger \sigma_- + a \sigma_+), \quad (19)$$

where $\sigma_\pm = (\sigma_x \pm i\sigma_y)/2$ are the atomic transition operators with the Pauli matrices $\sigma_{x,y,z}$. While a (a^\dagger)

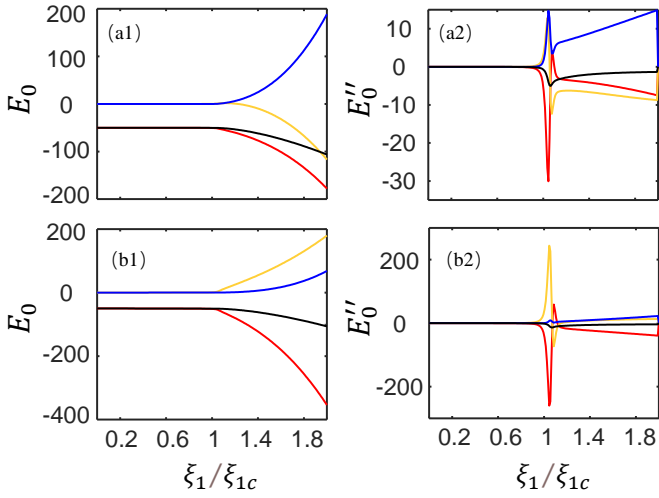


FIG. 5. (a1), (b1) Sum of patterns of ground state energy level (black solid line) and corresponding pattern components (red, yellow, and blue solid lines) as as functions of coupling strength ξ_1/ξ_{1c} when $k = 0.5$ and $k = 1.5$. (a2), (b2) Second-order derivatives of the corresponding energy levels (black solid line) and corresponding pattern components (red, yellow, and blue solid lines).

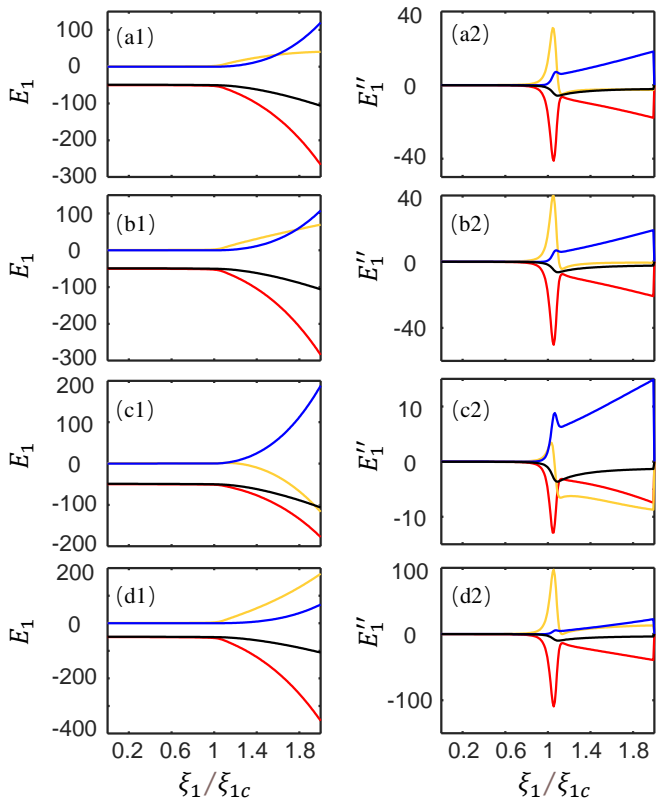


FIG. 6. (a1)-(d1) Sum of patterns of first excited state energy level (black solid line) and corresponding pattern components (red, yellow, and blue solid lines) as as functions of coupling strength ξ_1/ξ_{1c} when $k = 0.9, 1, 0.5$ and 1.5 . (a2)-(d2) Second-order derivatives of the corresponding energy levels (black solid line) and corresponding pattern components (red, yellow, and blue solid lines).

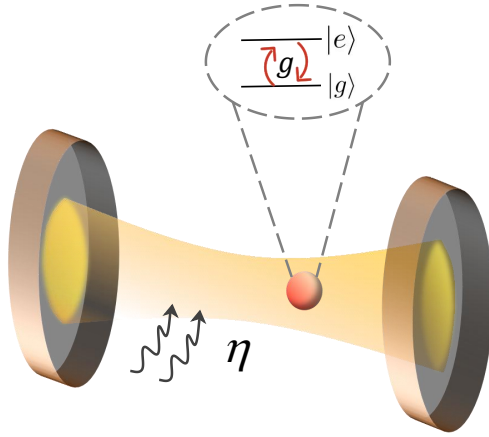


FIG. 7. Schematic of a qubit weakly coupled to a cavity driven by two-photon, with an amplitude η . The states $|g\rangle$ and $|e\rangle$ are the ground and excited states of the qubit, respectively. The qubit-cavity coupling strength is g .

is the annihilation (creation) operator of the cavity, η is the parametric drive amplitude and g is the qubit-cavity coupling strength. The $\delta_c = \omega_c - \omega_p/2$ is the cavity detuning, and $\delta_q = \omega_q - \omega_p/2$ is the qubit detuning (with ω_c and ω_q being the cavity and qubit frequencies, respectively).

The Hamiltonian H in Eq. (1) can be diagonalized by the squeezed operator $S(r) = \exp[r(a^2 - a^{\dagger 2})/2]$, where r is the squeezing parameter, defined by $\tanh 2r = \eta/\delta_c$. The squeezing transformation leads to

$$H_{\text{AR}} \equiv S(r)HS^{\dagger}(r) = H_0 + H_1, \quad (20)$$

where

$$\begin{aligned} H_0 &= \delta_c \operatorname{sech}(2r) a^{\dagger} a + \frac{\delta_q}{2} \sigma_z, \\ H_1 &= g_1(a\sigma_+ + a^{\dagger}\sigma_-) + g_2(a\sigma_- + a^{\dagger}\sigma_+). \end{aligned} \quad (21)$$

Here, $g_1 = g \cosh 2r$ and $g_2 = g \sinh 2r$ denote the qubit-cavity coupling strengths of the rotating-wave and counterrotating-wave interactions, respectively. The Hamiltonian H_{AR} in Eq. (20) is a simulated anisotropic Rabi Hamiltonian. It is distinctly different from the isotropic Rabi model with $g_1 = g_2$ which has been proven to exhibit the QPT phenomenon [3, 48].

We denote $|\uparrow(\downarrow)\rangle$ as eigenstates of the qubit, and Fock states $|m\rangle$ ($m = 0, 1, 2, 3, \dots$) as the states of the cavity. The Hamiltonian H_0 has decoupled spin subspaces $\Gamma_{(\downarrow)}$ and $\Gamma_{(\uparrow)}$. For $\delta_c \operatorname{sech}(2r)/\delta_q \rightarrow \infty$, the eigenstates of the lowest energy of H_0 correspond to the eigenstates of the resonator confined in $\Gamma_{(\downarrow)}$. However, the interaction Hamiltonian H_1 introduces the coupling between the two spin subspaces, which makes the virtual excitation between them alter the nature of the low-energy eigenstates and eigenenergies. Therefore, we employ the time-dependent perturbation method [49] to obtain the effective Hamiltonian, which has no coupling between $\Gamma_{(\downarrow)}$ and $\Gamma_{(\uparrow)}$.

In a frame rotating with $\frac{\delta_q}{2}\sigma_z$, the Hamiltonian H_{AR} becomes

$$H' = \delta_c \operatorname{sech}(2r) a^\dagger a + g_1 (a\sigma_+ e^{i\delta_q t} + a^\dagger \sigma_- e^{-i\delta_q t}) + g_2 (a\sigma_- e^{-i\delta_q t} + a^\dagger \sigma_+ e^{i\delta_q t}) + \frac{\delta_q}{2} \sigma_z, \quad (22)$$

then, according to the time-dependent perturbation method [49], the Hamiltonian H' in Eq. (22) can be written as

$$H_I = \delta_c \operatorname{sech}(2r) a^\dagger a + \frac{g_1^2 + g_2^2}{\delta_q} a^\dagger a \sigma_z + \left(\frac{g_1^2}{\delta_q} + \frac{\delta_q}{2} \right) \sigma_z + \frac{g_1 g_2}{\delta_q} (a^{\dagger 2} + a^2) \sigma_z + \frac{g_1^2 - g_2^2}{\delta_q} \sigma_- \sigma_+. \quad (23)$$

We use the same method as in Ref. [4] to derive the following quantities for both normal and superradiant phases: low-energy Hamiltonians, excitation energies, eigenvalues with corresponding eigenstates, and critical coupling strength. The low-energy effective Hamiltonian of the normal phase takes the form

$$H_{\text{np}} = \left(\delta_c \operatorname{sech}(2r) - \frac{g_1^2 + g_2^2}{\delta_q} \right) a^\dagger a - \frac{g_1 g_2}{\delta_q} (a^{\dagger 2} + a^2) - \frac{g_1^2}{\delta_q} - \frac{\delta_q}{2}. \quad (24)$$

The squeezing transformation $S'^\dagger(r'_{\text{np}}) H_{\text{np}} S'(r'_{\text{np}})$ yielding $H'_{\text{np}} = \epsilon_{\text{np}} a^\dagger a + E_{\text{np}}$, with the excitation energy

$$\epsilon_{\text{np}} = \sqrt{\left(\delta_c \operatorname{sech}(2r) - \frac{g^2 \cosh(2r)}{\delta_q} \right)^2 - \frac{g^4 \sinh^2(2r)}{\delta_q}}, \quad (25)$$

and the squeezing parameter

$$r'_{\text{np}} = \frac{1}{4} \ln \left[1 + \frac{2g^2 \sinh(2r)}{\delta_c \operatorname{sech}(2r) \delta_q - g^2 e^{2r}} \right]. \quad (26)$$

Then we obtain the critical coupling strength

$$g_c = \frac{g e^r}{\sqrt{\delta_c \operatorname{sech}(2r) \delta_q}} \leq 1, \quad (27)$$

the eigenstates and eigenvalues of H'_{np} are given by

$$|\phi_{\text{np}}^m\rangle = S'(r'_{\text{np}}) |m\rangle |\downarrow\rangle, \quad (28)$$

$$E_{\text{np}}^m = m \epsilon_{\text{np}} + E_{\text{np}}. \quad (29)$$

Likewise in the superradiant phase, we obtain the low-energy effective Hamiltonian

$$H_{\text{sp}} \simeq \left[\delta_c \operatorname{sech}(2r) - \frac{(g_1 + g_2)^2 g_c^{-4} + (g_1 - g_2)^2}{2\delta_q g_c^2} \right] a^\dagger a - \frac{(g_1 + g_2)^2 g_c^{-4} - (g_1 - g_2)^2}{4\delta_q g_c^2} (a^{\dagger 2} + a^2) - \frac{[(g_1 + g_2) g_c^{-2} - (g_1 - g_2)]^2}{4\Omega g_c^2} - \frac{\Omega g_c^{-2}}{2}, \quad (30)$$

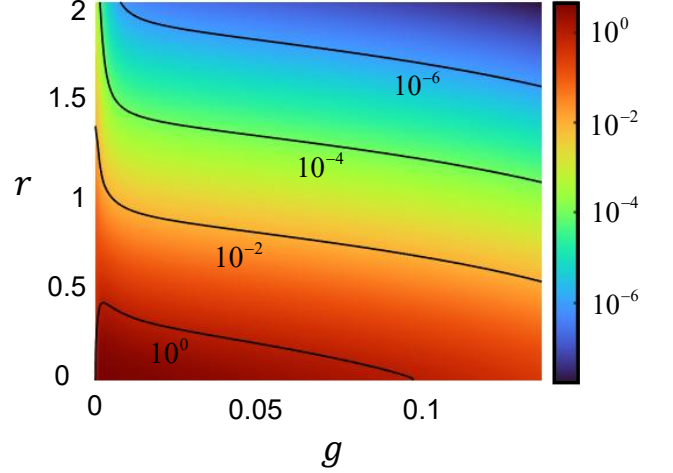


FIG. 8. Thermogram shows the distribution of the logarithmic value $\log(E_1 - E_0)$ of the energy gap between the excited state and the ground state in the parameter space (g, r) .

the excitation energy

$$\epsilon_{\text{sp}} = \sqrt{\left[\delta_c \operatorname{sech}(2r) - \frac{\delta_c \operatorname{sech}(2r) \delta_q g_c^{-2} + g^2 e^{-2r}}{2\delta_q g_c^2} \right]^2 - \left[\frac{\delta_c \operatorname{sech}(2r) \delta_q - g^2 e^{-2r}}{4\delta_q g_c^2} \right]^2}, \quad (31)$$

and the eigenstates and eigenenergies of H_{sp}

$$|\phi_{\text{sp}}^m\rangle = D(\pm\alpha_0) S'(r'_{\text{sp}}) |m\rangle |\downarrow^\pm\rangle, \quad (32)$$

where

$$r'_{\text{sp}} = \frac{1}{4} \ln \left[\frac{2g^2 \sinh(2r)}{g^2 e^{2r}} (1 - g_c^{-4})^{-1} \right], \quad (33)$$

$$|\downarrow^\pm\rangle = \mp \sqrt{\frac{1 - g_c^{-2}}{2}} |\uparrow\rangle + \sqrt{\frac{1 + g_c^{-2}}{2}} |\downarrow\rangle. \quad (34)$$

V. ANALYSIS OF QUANTUM PHASE TRANSITION

Under the weak coupling mechanism, we can control the occurrence of phase transitions by changing the two-photon driving strength. As shown in Fig. 8, when the coupling strength is within a certain range, as the squeezing parameter increases, the energy gap between the excited state and the ground state tends to zero, that is, the energy level undergoes degeneracy. Then, we analyze the characteristics of the system in both normal and superradiant phases when the squeezing parameter is set to be $r = \sqrt{2}$. The excitation energies ϵ_{np} and

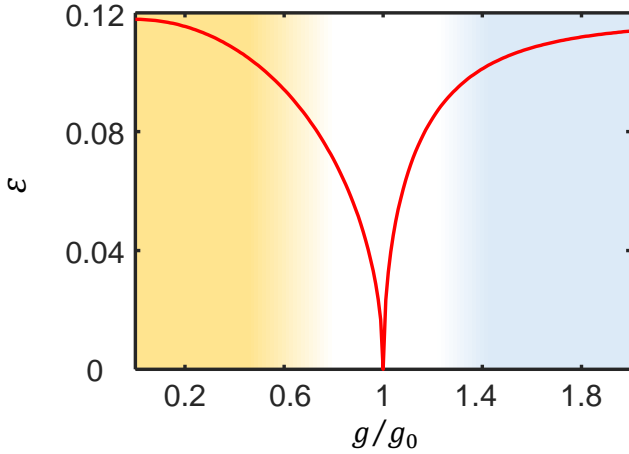


FIG. 9. Excitation energies of the anisotropic Rabi Hamiltonian as functions of the coupling strengths g/g_0 . We choose parameters $r = \sqrt{2}$ and we set $\delta_q = 200\delta_c \text{sech}(2r) = 23.56\delta_c$. The disappearance of ϵ at the critical point g/g_0 signifies the emergence of the QPT. Here, $g_0 = \sqrt{\delta_c \text{sech}(2r) \delta_q} / e^r$.

ϵ_{sp} that can characterize the behavior of the system as a function of coupling strength g/g_0 are shown in Fig. 9.

The numerical results indicate that the excitation energy in both normal and superradiant phases vanishes as the coupling strength approaches the critical point. The ground-state energy as a function of coupling strength g/g_0 has displayed in Fig. 10(a) and second derivative of ground-state energy $d^2E_G/d^2(g/g_0)$ as a function of coupling strength g/g_0 has displayed in Fig. 10(b). From Fig. 10, we see that the ground-state energy decreases at the critical point $g/g_0 = 1$, and it follows a continuous curve. While $d^2E_G/d^2(g/g_0)$ displays a discontinuity at the critical point $g/g_0 = 1$, which clearly indicates the second-order nature of the QPT. Moreover, this discontinuity becomes more pronounced as the squeezing parameter r increases. The photon number in the squeezed picture $N_c = \langle a^\dagger a \rangle$, which is the order parameter of QPT, is presented in Fig. 11. For $g/g_0 < 1$, i.e., in the normal phase, the photon number n_c is zero, while for $g/g_0 > 1$, i.e., in the superradiant phase, the photon number N_c becomes infinity. This indicates that when $g/g_0 > 1$, the photon number N_c acquires macroscopic occupations.

VI. CONCLUSION

In conclusion, we obtained three patterns by diagonalizing the anisotropic Rabi model in operator space and simulated the contribution of three patterns to the ground state and excited state. The results show that the three patterns are in competition during the superradiant phase transition. That is, with the increase of coupling strength, (i) the pattern λ_1 drives the phase transition; (ii) the pattern λ_2 has a similar

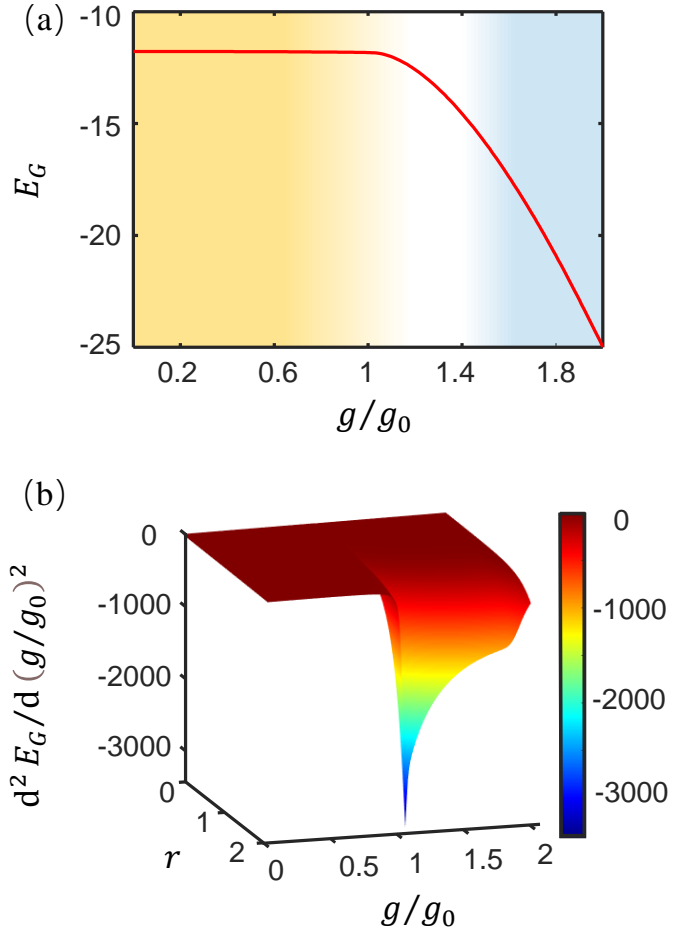


FIG. 10. (a) Ground-state energy E_G as the function of the coupling strengths g/g_0 . (b) The second derivative of ground-state energy $d^2E_G/d(g/g_0)^2$ as the function of the coupling strengths g/g_0 . We choose parameters $r = \sqrt{2}$ and we set $\delta_q = 200\delta_c \text{sech}(2r) = 23.56\delta_c$. Here, $g_0 = \sqrt{\delta_c \text{sech}(2r) \delta_q} / e^r$.

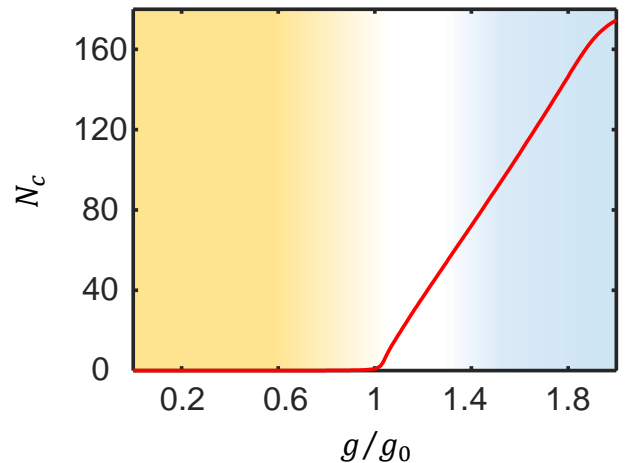


FIG. 11. Photon number of the anisotropic Rabi Hamiltonian as functions of the coupling strengths g/g_0 . We choose parameters $r = \sqrt{2}$ and we set $\delta_q = 200\delta_c \text{sech}(2r) = 23.56\delta_c$. The nonzero N_c at the critical point $g/g_0 = 1$ indicates the occurrence of the QPT. Here, $g_0 = \sqrt{\delta_c \text{sech}(2r) \delta_q} / e^r$.

response speed to compensate for the pattern λ_1 , but the energy compensation is less than the pattern λ_1 ; (iii) the pattern λ_3 shows a slow response speed, but plays a key role in balancing the pattern λ_1 . This competitive relationship explains why and how the superradiant phase transition occurs. We also explore how different ratios of the rotating-wave to counter-rotating-wave coupling strengths affect pattern competition. In addition, we propose a protocol, using a parametrically-driven Jaynes-Cummings model to explore the quantum phase transition. In the squeezed-light frame, this parametrically-driven Jaynes-Cummings model can accurately simulate the dynamics of an ultrastrong-coupling anisotropic Rabi model. The results of numerical simulations demonstrate that this anisotropic Rabi model undergoes a quantum phase transition at the critical point $g/g_0 \sim 1$. To be specific, as the coupling strength approaches the critical point, the excitation energy tends to zero; The ground-state energy is continuous at the critical point, while its second derivative to the coupling strength is discontinuous at

the critical point; When the coupling strength exceeds the critical point, the photon number increases to infinity. Our work provides a deeper understanding of the microscopic mechanisms behind the superradiant phase transition in the anisotropic quantum Rabi model, and offers a theoretical framework for the realization of controllable quantum phase transitions.

ACKNOWLEDGEMENTS

Y.-H.C. was supported by the National Natural Science Foundation of China under Grant No. 12304390 and 12574386, the Fujian 100 Talents Program, and the Fujian Minjiang Scholar Program. Y. X. was supported by the National Natural Science Foundation of China under Grant No. 62471143, the Key Program of National Natural Science Foundation of Fujian Province under Grant No.2024J02008, and the project from Fuzhou University under Grant No. JG2020001-2.

[1] L. D. Landau, On the theory of phase transitions. I., *Phys. Z. Sowjet.* **11**, 26 (1937).

[2] L. Carr, *Understanding Quantum Phase Transitions* (CRC Press, 2010) p. 756.

[3] M.-J. Hwang, R. Puebla, and M. B. Plenio, Quantum phase transition and universal dynamics in the Rabi model, *Phys. Rev. Lett.* **115**, 180404 (2015).

[4] L.-T. Shen, Z.-B. Yang, H.-Z. Wu, and S.-B. Zheng, Quantum phase transition and quench dynamics in the anisotropic Rabi model, *Phys. Rev. A* **95**, 013819 (2017).

[5] M.-J. Hwang and M. B. Plenio, Quantum phase transition in the finite Jaynes-cummings lattice systems, *Phys. Rev. Lett.* **117**, 123602 (2016).

[6] R.-H. Zheng, W. Ning, Y.-H. Chen, J.-H. Lü, L.-T. Shen, K. Xu, Y.-R. Zhang, D. Xu, H. Li, Y. Xia, F. Wu, Z.-B. Yang, A. Miranowicz, N. Lambert, D. Zheng, H. Fan, F. Nori, and S.-B. Zheng, Observation of a superradiant phase transition with emergent cat states, *Phys. Rev. Lett.* **131**, 113601 (2023).

[7] M. Vojta, R. Bulla, and W. Hofstetter, Quantum phase transitions in models of coupled magnetic impurities, *Phys. Rev. B* **65**, 140405 (2002).

[8] Y. Kleeorin and Y. Meir, Quantum phase transition in a realistic double-quantum-dot system, *Sci. Rep.* **8**, 10539 (2018).

[9] F. J. González, A. Norambuena, and R. Coto, Dynamical quantum phase transition in diamond: Applications in quantum metrology, *Phys. Rev. B* **106**, 014313 (2022).

[10] Y. Zhang, B.-B. Mao, D. Xu, Y.-Y. Zhang, W.-L. You, M. Liu, and H.-G. Luo, Quantum phase transitions and critical behaviors in the two-mode three-level quantum rabi model, *J. Phys. A: Math. Theor.* **53**, 315302 (2020).

[11] C. J. Zhu, L. L. Ping, Y. P. Yang, and G. S. Agarwal, Squeezed light induced symmetry breaking superradiant phase transition, *Phys. Rev. Lett.* **124**, 073602 (2020).

[12] C. Emary and T. Brandes, Chaos and the quantum phase transition in the Dicke model, *Phys. Rev. E* **67**, 066203 (2003).

[13] F. Dimer, B. Estienne, A. Parkins, and H. Carmichael, Proposed realization of the Dicke-model quantum phase transition in an optical Cavity QED System, *Phys. Rev. A* **75**, 013804 (2006).

[14] Y. K. Wang and F. T. Hioe, Phase transition in the Dicke model of superradiance, *Phys. Rev. A* **7**, 831 (1973).

[15] V. M. Bastidas, C. Emary, B. Regler, and T. Brandes, Nonequilibrium quantum phase transitions in the Dicke model, *Phys. Rev. Lett.* **108**, 043003 (2012).

[16] D. Tolokunov and D. Solenov, Quantum phase transition in the multimode Dicke model, *Phys. Rev. B* **75**, 024402 (2007).

[17] D. Nagy, G. Kónya, G. Szirmai, and P. Domokos, Dicke-model phase transition in the quantum motion of a Bose-Einstein Condensate in an Optical Cavity, *Phys. Rev. Lett.* **104**, 130401 (2010).

[18] C. M. Bowden and C. C. Sung, First- and second-order phase transitions in the Dicke model: Relation to optical bistability, *Phys. Rev. A* **19**, 2392 (1979).

[19] L. Bakemeier, A. Alvermann, and H. Fehske, Quantum phase transition in the Dicke model with critical and noncritical entanglement, *Phys. Rev. A* **85**, 043821 (2012).

[20] N. Lambert, C. Emary, and T. Brandes, Entanglement and the phase transition in single-mode superradiance, *Phys. Rev. Lett.* **92**, 073602 (2004).

[21] K. Hepp and E. H. Lieb, On the superradiant phase transition for molecules in a quantized radiation field: the Dicke maser model, *Ann. Phys.* **76**, 360 (1973).

[22] Y. K. Wang and F. T. Hioe, Phase transition in the Dicke model of superradiance, *Phys. Rev. A* **7**, 831 (1973).

[23] M. O. Scully, Single photon subradiance: Quantum control of spontaneous emission and ultrafast readout, *Phys. Rev. Lett.* **115**, 243602 (2015).

[24] N. Shammah *et al.*, Open quantum systems with local and collective incoherent processes: Efficient numerical

simulations using permutational invariance, *Phys. Rev. A* **98**, 063815 (2018).

[25] C. Emary and T. Brandes, Quantum chaos triggered by precursors of a quantum phase transition: The Dicke model, *Phys. Rev. Lett.* **90**, 044101 (2003).

[26] R. Puebla, M.-J. Hwang, and M. B. Plenio, Excited-state quantum phase transition in the Rabi model, *Phys. Rev. A* **94**, 023835 (2016).

[27] J. Liu, M. Zhao, Y.-T. Yang, and H.-G. Luo, Using nonclassical states to explore the superradiant phase transition in the quantum Rabi model, *Phys. Rev. A* **109**, 023721 (2024).

[28] M. Cai, Z. Liu, W. Zhao, Y. Wu, Q. Mei, Y. Jiang, L. He, X. Zhang, Z. Zhou, and L. Duan, Observation of a quantum phase transition in the quantum rabi model with a single trapped ion, *Nat. Commun.* **12**, 1126 (2021).

[29] R.-H. Zheng *et al.*, Observation of a superradiant phase transition with emergent cat states, *Phys. Rev. Lett.* **131**, 113601 (2023).

[30] Z.-J. Ying *et al.*, Quantum phase transition and spontaneous symmetry breaking in a nonlinear quantum rabi model, *J. Phys. A: Math. Theor.* **51**, 315302 (2018).

[31] L.-T. Shen, J.-W. Yang, Z.-R. Zhong, and Z.-B. Yang, Quantum phase transition and quench dynamics in the two-mode Rabi model, *Phys. Rev. A* **104**, 063703 (2021).

[32] S. Ashhab, Superradiance transition in a system with a single qubit and a single oscillator, *Phys. Rev. A* **87**, 013826 (2013).

[33] X. Chen, Z. Wu, M. Jiang, *et al.*, Experimental quantum simulation of superradiant phase transition beyond no-go theorem via antisqueezing, *Nat. Commun.* **12**, 6281 (2021).

[34] Q.-T. Xie, S. Cui, J.-P. Cao, L. Amico, and H. Fan, Anisotropic Rabi model, *Phys. Rev. X* **4**, 021046 (2014).

[35] G. Zhang and H. Zhu, Analytical solution for the anisotropic rabi model: Effects of counter-rotating terms, *Sci. Rep.* **5**, 8756 (2015).

[36] P. Nataf and C. Ciuti, No-go theorem for superradiant quantum phase transitions in cavity qed and counterexample in circuit qed, *Nat. Commun.* **1**, 72 (2010).

[37] R. Puebla, A. Relaño, and J. Retamosa, Excited-state phase transition leading to symmetry-breaking steady states in the dicke model, *Phys. Rev. A* **87**, 023819 (2013).

[38] D. Lamberto, G. Orlando, and S. Sawasta, Superradiant quantum phase transition in open systems: System-bath interaction at the critical point, *Phys. Rev. A* **100**, 063815 (2024).

[39] K. Rzażewski, K. Wódkiewicz, and W. Zakowicz, Phase transitions, two-level atoms, and the a^2 term, *Phys. Rev. Lett.* **35**, 432 (1975).

[40] B. W. Shore and P. L. Knight, The Jaynes-Cummings model, *J. Mod. Opt.* **40**, 1195–1238 (1993).

[41] J.-F. Huang, J.-Q. Liao, and L.-M. Kuang, Ultrastrong Jaynes-Cummings model, *Phys. Rev. A* **101**, 043835 (2020).

[42] W. Qin, A. Miranowicz, P.-B. Li, X.-Y. Lü, J. You, and F. Nori, Exponentially enhanced light-matter interaction, cooperativities, and steady-state entanglement using parametric amplification, *Phys. Rev. Lett.* **120** (2018).

[43] C. Leroux, L. C. G. Govia, and A. A. Clerk, Enhancing cavity quantum electrodynamics via antisqueezing: Synthetic ultrastrong coupling, *Phys. Rev. Lett.* **120**, 093602 (2018).

[44] Y.-H. Chen, W. Qin, X. Wang, A. Miranowicz, and F. Nori, Shortcuts to adiabaticity for the quantum Rabi model: Efficient generation of giant entangled cat states via parametric amplification, *Phys. Rev. Lett.* **126**, 023602 (2021).

[45] W. Qin, Y.-H. Chen, X. Wang, A. Miranowicz, and F. Nori, Strong spin squeezing induced by weak squeezing of light inside a cavity, *Nanophotonics* **9**, 4853–4868 (2020).

[46] Y.-T. Yang and H.-G. Luo, Dissecting superradiant phase transition in the quantum Rabi model, *Chin. Phys. Lett.* **41**, 120501 (2024).

[47] X. Wang and H.-R. Li, Chiral quantum network with giant atoms, *Quant. Sci. Tech.* **7**, 035007 (2022).

[48] Y.-H. Chen, Y. Qiu, A. Miranowicz, N. Lambert, W. Qin, R. Stassi, Y. Xia, S.-B. Zheng, and F. Nori, Sudden change of the photon output field marks phase transitions in the quantum rabi model, *Commun. Phys.* **7**, 5 (2024).

[49] W. Shao, C. Wu, and X.-L. Feng, Generalized James' effective hamiltonian method, *Phys. Rev. A* **95**, 032124 (2017).